

Compact single mode tunable laser using a digital micromirror device

Frank Havermeier,¹ Lawrence Ho,¹ and Christophe Moser^{2,*}

¹Ondax Inc., 850 E. Duarte Road, Monrovia, CA 91016, USA

²Laboratory of Applied Photonics Devices, School of Engineering, Swiss Federal Institute of Technology Lausanne (EPFL) Switzerland

*christophe.moser@epfl.ch

Abstract: The wavelength tuning properties of a tunable external cavity laser based on multiplexed volume holographic gratings and a commercial micromirror device are reported. The 3x3x3 cm³ laser exhibits single mode operation in single or multi colors between 776 nm and 783 nm with less than 7.5 MHz linewidth, 37 mW output power, 50 μ s rise/fall time constant and a maximum switching rate of 0.66 KHz per wavelength. The unique discrete-wavelength-switching features of this laser are also well suited as a source for continuous wave Terahertz generation and three-dimensional metrology.

©2011 Optical Society of America

OCIS codes: (140.0140) Lasers and laser optics; (140.3600) lasers tunable.

References and links

1. M. C. Wu, A. Solgaard, and J. E. Ford, "Optical MEMS for lightwave communication," *J. Lightwave Technol.* **24**(12), 4433–4454 (2006).
2. W. Huang, R. R. A. Syms, J. Staggs, and A. Lohmann, "Precision MEMS flexure mount for a Littman tunable external cavity laser," *IEE Proc. Scie. Meas. Technol.* **151**(2), 67–75 (2004).
3. R. R. A. Syms and A. Lohmann, "MOEMS tuning element for a Littrow external cavity laser," *J. Microelectromech. Syst.* **12**(6), 921–928 (2003).
4. X. M. Zhang, A. Q. Liu, C. Lu, and D. Y. Tang, "Continuous wavelength tuning in micromachined Littrow external-cavity lasers," *IEEE J. Quantum. Electron.* **41**(2), 187–197 (2005).
5. J. D. Berger, Y. W. Zhang, J. D. Grade, H. Lee, S. Hriaya, H. Jerman, A. Fennema, A. Tselikov, and D. Anthon, "Widely tunable external cavity diode laser using a MEMS electrostatic rotary actuator," *Ecoc'01: 27th European Conference on Optical Communication, Vols 1–6*, 198–199 (2001).
6. M. Breede, S. Hoffmann, J. Zimmermann, J. Struckmeier, M. Hofmann, T. Kleine-Ostmann, P. Knobloch, M. Koch, J. P. Meyn, M. Matus, S. W. Koch, and J. V. Moloney, "Fourier-transform external cavity lasers," *Opt. Commun.* **207**(1–6), 261–271 (2002).
7. M. Breede, C. Kasseck, C. Brenner, N. C. Gerhardt, M. Hofmann, and R. Hofling, "Micromirror device controlled tunable diode laser," *Electron. Lett.* **43**(8), 456–457 (2007).
8. B. B. Hu and M. C. Nuss, "Imaging with terahertz waves," *Opt. Lett.* **20**(16), 1716 (1995).
9. K. J. Siebert, H. Quast, R. Leonhardt, T. Löffler, M. Thomson, T. Bauer, H. G. Roskos, and S. Czasch, "Continuous-wave all-optoelectronic terahertz imaging," *Appl. Phys. Lett.* **80**(16), 3003–3005 (2002).
10. E. Pickwell and V. P. Wallace, "Biomedical applications of terahertz technology," *J. Phys. D Appl. Phys.* **39**(17), R301–R310 (2006).
11. T. Kleine-Ostmann, P. Knobloch, M. Koch, S. Hoffmann, M. Breede, M. Hofmann, G. Hein, K. Pierz, M. Sperling, and K. Donhuijsen, "Continuous-wave THz imaging," *Electron. Lett.* **37**(24), 1461–1463 (2001).
12. K. Kawase, Y. Ogawa, Y. Watanabe, and H. Inoue, "Non-destructive terahertz imaging of illicit drugs using spectral fingerprints," *Opt. Express* **11**(20), 2549–2554 (2003).
13. C. Jansen, S. Wietzke, O. Peters, M. Scheller, N. Vieweg, M. Salhi, N. Krumbholz, C. Jordens, T. Hochrein, and M. Koch, "Terahertz imaging: applications and perspectives," *Appl. Opt.* **49**(19), E48–E57 (2010).
14. C. Moser, L. Ho, and F. Havermeier, "Self-aligned non-dispersive external cavity tunable laser," *Opt. Express* **16**(21), 16691–16696 (2008).
15. G. J. Steckman, W. Liu, R. Platz, D. Schroeder, C. Moser, and F. Havermeier, "Volume holographic grating wavelength stabilized laser diodes," *IEEE J. Sel. Top. Quant.* **13**(3), 672–678 (2007).
16. O. M. Efimov, L. B. Glebov, L. N. Glebova, K. C. Richardson, and V. I. Smirnov, "High-efficiency bragg gratings in photothermorefractive glass," *Appl. Opt.* **38**(4), 619–627 (1999).
17. C. Moser and G. Steckman, "Filters to Bragg about," *Photon. Spectra* **39**, 82 (2005).
18. H. Kogelnik, "Coupled Wave Theory for Thick Hologram Gratings," *Bell Syst. Tech. J.* **48**, 2909 (1969).

19. C. S. Friedrich, C. Brenner, S. Hoffmann, A. Schmitz, I. C. Mayorga, A. Klehr, G. Erbert, and M. R. Hofmann, "New two-color laser concepts for THz generation," *IEEE J. Sel. Top. Quant.* **14**(2), 270–276 (2008).
20. M. Matus, M. Kolesik, J. V. Moloney, M. Hofmann, and S. W. Koch, "Dynamics of two-color laser systems with spectrally filtered feedback," *J. Opt. Soc. Am. B* **21**(10), 1758–1771 (2004).
21. J. R. Demers, R. T. Logan, N. J. Bergeron, and E. R. Brown, "A High Signal-to-Noise Ratio, Coherent, Frequency-Domain THz Spectrometer Employed to Characterize Explosive Compounds," 2008 33rd International Conference on Infrared, Millimeter and Terahertz Waves, Vols 1 and 2, 234–236 (2008).
22. J. R. Demers, R. T. Logan, and E. R. Brown, "An optically integrated coherent frequency-domain THz spectrometer with signal-to-noise ratio up to 80 dB," 2007 International Topical Meeting on Microwave Photonics, 92–95 (2007).
23. J. R. Demers, R. T. Logan, N. J. Bergeron, and E. R. Brown, "A coherent frequency-domain THz spectrometer with a signal-to-noise ratio 60 dB at 1 THz - art. no. 694909," *Terahertz for Military and Security Applications Iv* **6949**, 94909–94909 (2008).
24. A. J. Deninger, T. Gobel, D. Schönherr, T. Kinder, A. Roggenbuck, M. Koberle, F. Lison, T. Muller-Wirts, and P. Meissner, "Precisely tunable continuous-wave terahertz source with interferometric frequency control," *Rev. Sci. Instrum.* **79**(4), 044702 (2008).
25. J. Kuhn, T. Colomb, F. Montfort, F. Charriere, Y. Emery, E. Cuche, P. Marquet, and C. Depeursinge, "Real-time dual-wavelength digital holographic microscopy with a single hologram acquisition," *Opt. Express* **15**(12), 7231–7242 (2007).
26. C. C. Aleksoff, "Multi-Wavelength digital holographic metrology - art. no. 63111D," *Opt. Info. Syst. IV* **6311**, D3111–D3111 (2006).

1. Introduction

The use of digital micromirror (MEMS) devices can offer both size and speed advantages in the application of spectral tuning of external cavity lasers, when compared to current mechanical actuators. The low mass of the micromirrors enables extremely rapid response, and their small size provides ample opportunities for additional integration into compact laser systems [1]. Several mode-hop-free tunable external laser architectures have been previously proposed by Academic research teams with analog micromirrors, which provide a continuous range of angular or linear motion in Littman [2] and Littrow [3, 4] implementations, leading to a continuous wavelength sweep. Additionally, a continuously-tunable laser (based on a MEMS electrostatic actuator in a Littman/Metcalf implementation) was developed commercially for telecommunication at 1.5 micrometers [5]. However, analog optical MEMS actuators are costly unless they are mass-produced. Consequently, all commercial widely tunable lasers operating outside the telecommunication window (1.5 μm) use bulky mechanical actuators that compromise both speed and integration.

An interesting approach reported by Breede et al. [6, 7] is to make use of inexpensive digital micromirrors, such as those found in DLP (digital light projector) display elements (e.g. Texas Instruments), in order to spectrally tune a laser. In their implementation, a lens transforms the spectrum (angularly spread by a diffraction grating) into a spatially spread spectrum at the Fourier plane of the lens. Unfortunately, the combination of the finite pixel size of DLP micromirrors (10–15 μm) and the reported long focal length (150 mm) of the lens necessary to spread the spectrum make it impossible to obtain single mode operation of the laser. The compactness of the laser system is also compromised since the length of the laser becomes at least twice the focal length of the lens.

Here, we demonstrate a tunable laser implementation with a micromirror array that provides for *both* single mode operation (with either single line or multi-lines), *and* a very compact overall size: $3 \times 3 \times 3 \text{ cm}^3$. This approach can enable new, portable, low-cost photonic systems in a variety of applications, including discretely tunable continuous wave Terahertz generation via difference frequency generation. This has applications in bio-medical imaging [8–11], imaging of hidden illicit drugs [12], and industrial imaging [13], among many others.

The manuscript is organized as follows:

- Section 2: Architecture of the external cavity laser
- Section 3: Discussion of the wavelength selective element of the external laser cavity.

- Section 4: Description of the digital micromirror array.
- Section 5: Laser wavelength tuning results
- Section 6: Potential capabilities of the technology

2. Laser external cavity architecture

The laser external cavity is based on a degenerate self-aligned cavity with a volume holographic grating as the wavelength selective element [14]. The set-up is illustrated in Fig. 1.

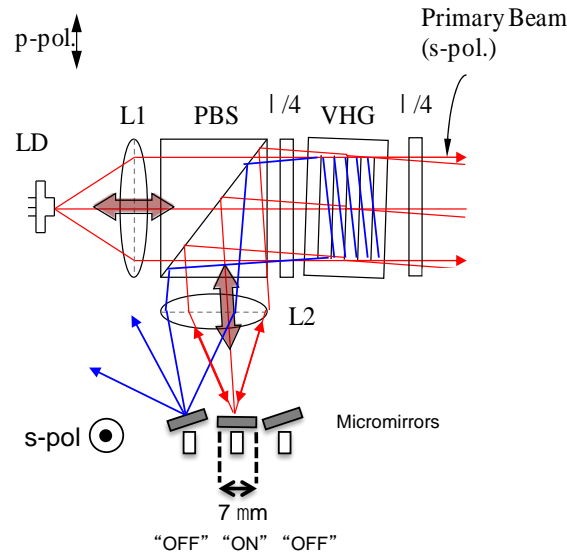


Fig. 1. Tunable laser cavity implemented with a micromirror array with two discrete wavelengths represented by the red and blue paths reflected from the VHG. LD: laser diode, VHG: volume holographic grating, PBS: polarizing beam-splitter, $\lambda/4$: quarter-wave plate

The p -polarized beam from the laser diode LD (Eagleyard) is collimated by lens L1 and propagates through the polarizing beam splitter PBS. The reflective volume holographic grating VHG of length t operates in the Bragg regime and diffracts a specific wavelength of the beam at a specific angle. The diffracted beam is s -polarized after a double pass through the quarter-wave plate $\lambda/4$. The diffracted s -polarized beam is then reflected by the PBS towards a second lens L2 that focuses the beam onto an array of micromirrors placed at the focal plane of lens L2. The back facet of the laser diode LD and the micromirrors form the resonant cavity (the front facet of the laser diode is anti-reflection coated with reflectivity $R < 10^{-3}$). For a suitable orientation of the micromirror (shown as the middle mirror in Fig. 1 for illustration purposes) the beam is retroreflected. The retroreflected beam is then re-collimated by lens L2, reflected by the PBS and incident on the VHG at precisely the same angle it was first diffracted. This produces a second diffracted beam that is exactly counter-propagating with the initial collimated beam. A second pass through the quarter-wave plate $\lambda/4$ restores the polarization to p that is transmitted through the PBS and focused into the laser diode. The output coupler of the cavity is the VHG. The undiffracted beam, i.e zero order, is the output beam of the cavity. This resonant cavity is self-aligned because it is independent of the spatial and angular position of the wavelength selective element (VHG). In practice, the angular alignment of the mirror array is insensitive to within several degrees. The axial distance sensitivity is of the order of the rayleigh length of the focused beam [14].

3. Wavelength selective component: volume holographic grating

The VHG is multiplexed, i.e. the element contains superimposed volume phase gratings in the bulk. Each individual grating has a specific period Λ and orientation given by the slant angle ϕ . Two multiplexed gratings are shown schematically in Fig. 2 for illustration. The diffracted

output angle θ_{out} is related to the input angle θ_{in} by the relation: $\sin \theta_{out} = \sin \theta_{in} - \frac{\lambda}{\Lambda \cdot n} \sin \phi$

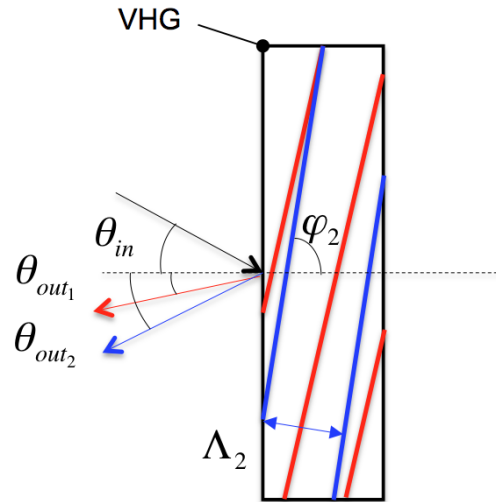


Fig. 2. Multiplexed reflective volume gratings

The multiplexed VHG therefore produces multiple diffracted beams from a multi-wavelength input beam, with each diffracted beam having a specific wavelength and output angle. These two parameters can be designed arbitrarily by changing the grating period and slant angle during the recording of the grating.

The diffracted output beam angle is mapped onto a linear position in the focal plane of lens L2 at the location of the micromirror array. For small diffracted angles $\theta_{out,i}$, $i = 1 \dots N$, N being the number of multiplexed gratings, the lateral position Δx in the focal plane is equal to $f \cdot \theta_{out,i}$ where f is the focal length of lens L2. A multiplexed volume grating was fabricated in a photothermal glass [15–17], with the parameters shown in Table 1.

Table 1. Functional Parameters of the Fabricated Multiplexed Volume Holographic Grating

Grating #	Wavelength [nm]	Slant ϕ [deg]	Diffraction angle θ_{out} [deg]	Diffraction efficiency [%]	Lateral position at focal place Δx [μm]
1	783.48	-0.17	-0.501	50 ± 5	-54.6
2	780.08	-0.02	-0.048	50 ± 5	-5.2
3	778.43	0.06	0.182	50 ± 5	19.8
4	776.73	0.14	0.408	50 ± 5	44.4

Note that the choice of multiplexed wavelengths was purely arbitrary. Any combination of wavelengths could have been multiplexed with the same physical separation of pixels on the DLP.

4. Micromirror array

A DLP micromirror array 1264 x 768 from Texas Instruments was obtained from a commercial projector. The mirror pixel size was not specified but was estimated to be $10\ \mu\text{m} \times 10\ \mu\text{m}$. The DLP is connected to the board by a flexible cable, which enabled alignment of the DLP in the laser cavity. The micromirrors were activated by sending a binary image to the DLP through a control board. The individual pixels of the binary image determine the “on” or “off” state of the corresponding micromirrors.

Figure 3(a) shows the orientation of the micromirrors when a “black” image was presented to the DLP and Fig. 3(b) shows the orientation of the micromirrors with a “white” image. Only binary images were used in order to maintain the mirrors in one of the two states (i.e. +12 degrees for “off” and -12 degrees for “on”).

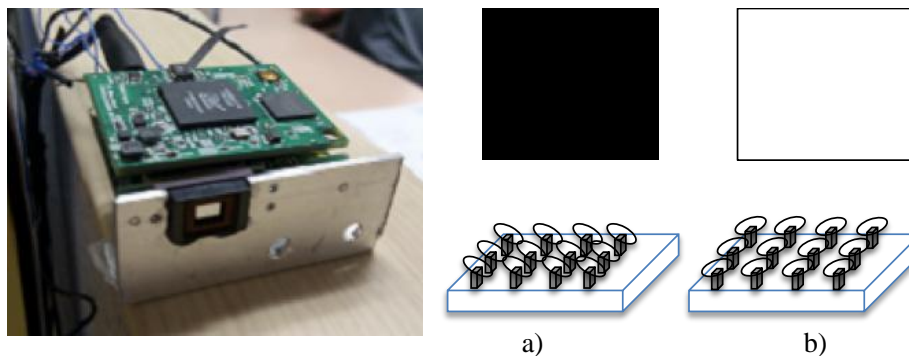


Fig. 3. DLP micromirror array. (a) top “black” image displayed to DLP corresponding to micromirrors oriented at +12 degrees from the normal: “off” state. (b) top “white” image corresponding to micromirrors oriented at -12 degrees from the normal: “on” state

The plane of deflection of this DLP is the plane formed by the normal to the micromirrors and one side of the DLP array. The DLP array was placed at the focal plane of lens L2 at an angle of -12 degrees such that the micromirrors are normal to the optical axis of the focusing lens and thus contributing optical feedback.

According to Table 1 (see lateral position at focal plane), the separation of the four wavelengths on the DLP array spanned 100 micrometers, or 10 pixels. The shortest separation between two wavelengths is therefore equal to 2 pixels. The reflectivity of the DLP, including the protective glass plate was 60% at 780 nm so the amount of feedback into the laser is approximately 15% for each selected wavelength.

5. DLP laser experimental results

A prototype switchable laser with the VHG and DLP was assembled. A picture of the assembled laser is shown in Fig. 4. All components except the DLP are mounted on a 20 mm x 20 mm thermoelectric cooler (TEC) so that temperature was controlled to within 0.04°C . The multiplexed VHG was mounted on a rotation system, whose pivot point is shown in Fig. 4. Rotation of the VHG provided fine wavelength tuning of 0.4 nm for 2 degrees rotation as the graph in Fig. 4 illustrates. Fine wavelength tuning was discontinuous because of the voids between the micromirror pixels: at the void, there is no feedback and thus no laser output. Due to the high fill factor of the array, 90% of the angle range between 0 and 2 degrees yielded a lasing external cavity.

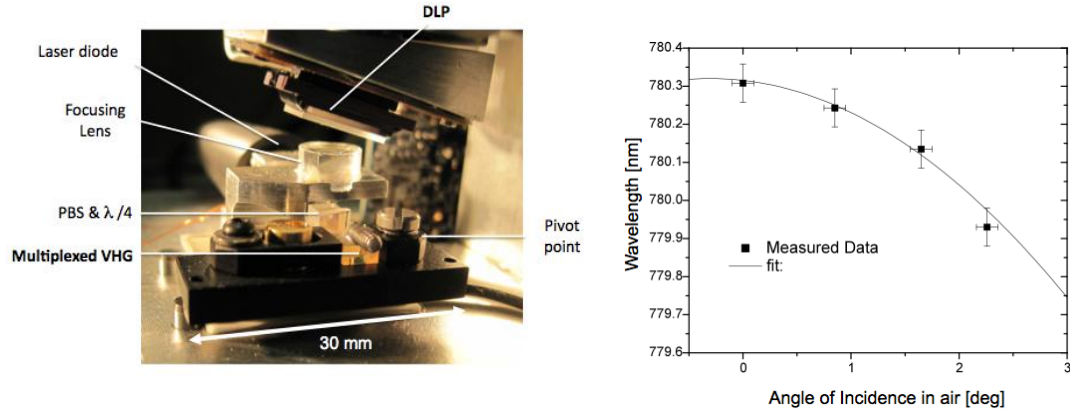


Fig. 4. Picture of the assembled DLP wavelength tunable laser and fine wavelength tuning by angle for the 780 nm line.

Figure 5 (a-d) shows the results of the tests. Each figure comprises the laser spectrum (EXFO/Burleigh WA1500), the binary image displayed on the DLP (top right) and the output beams (bottom right). The primary output beam is the bright spot in the image. The fainter spot is the secondary output beam, which is obtained after double diffraction off the VHG. The direction of the secondary output beam depends on the wavelength, whereas the direction of the primary output beam remains constant. In each figure (a-d), the abscissa of the “white” line, in the image presented to the DLP (top right), increases successively. The pixels forming the “white” line in the image displayed to the DLP correspond to the activation (“on”) of the corresponding line of pixels in the micromirror array.

The laser oscillated with a stable, single mode for each of the 4 wavelengths. The linewidth was measured with a scanning Fabry-Perot etalon (Thorlabs SA-200-6A). The linewidth measurement was limited by the resolution of the instrument to 7.5 MHz.

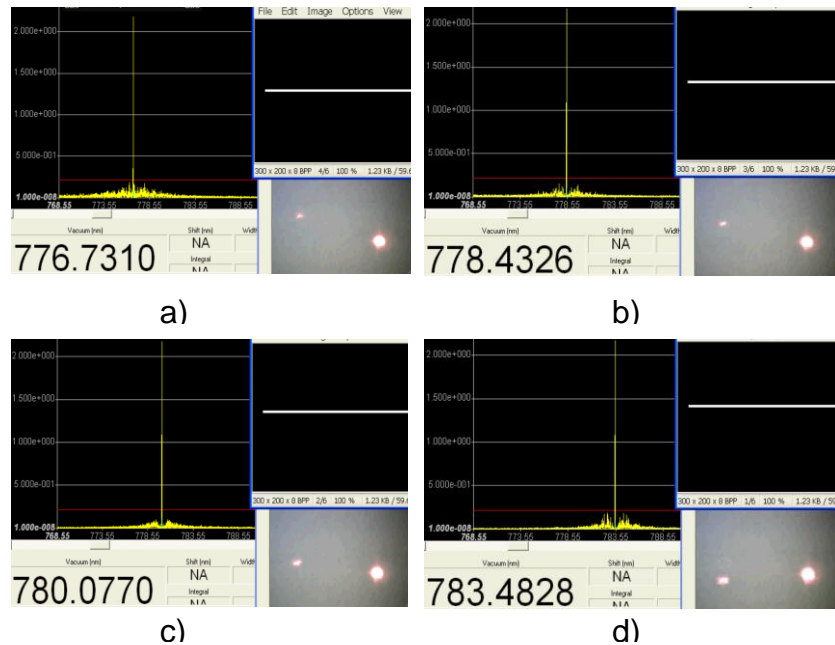


Fig. 5. Wavelength switching results of the prototype: (a-d) laser spectrum, displayed image on the DLP (top right), primary and secondary output laser beams (primary = bright spot).

When multiple pixels of the micromirror array, corresponding to different wavelengths, were switched “on”, the laser operated multi-line, however each laser line operated in single mode (Fig. 6).

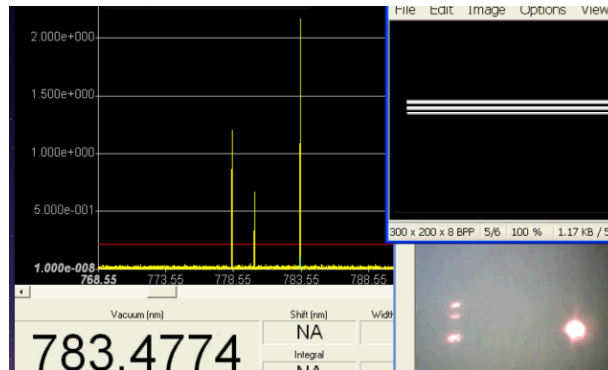


Fig. 6. Multi-line operation while maintaining single mode for each line

At maximum current, the output power in the primary beam reached 37 mW. A graph showing optical power versus input current for the 780 nm line is shown in Fig. 7. The kinks in the curve represent single mode hops.

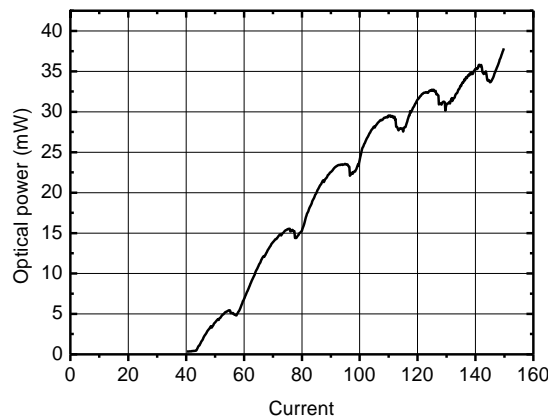


Fig. 7. Optical power versus current for the 780 nm line at 25°C.

The laser was driven at 83 mA for all subsequent measurements, well below the maximum current in order to avoid unwanted potential damage.

5.1 Wavelength switching dynamics

The wavelength switching dynamics of the laser were investigated by monitoring the power of the secondary output beam with a photodetector while the laser was switched between two wavelengths. Two photodetectors were used to detect the secondary output beams, one for each wavelength. The internal pulse width modulation (PWM) of the DLP was used in this experiment to dither the “white” lines of pixels.

[Note: PWM is used by the projector (from which the DLP has been extracted) to display colors. The full color refresh cycle of the DLP is approximately 7.5 ms. Within each cycle, the DLP can display 5 successive colored images. Therefore the time between wavelength switching is 1.5 ms, corresponding to one fifth the full DLP refresh rate (7.5 ms).]

Figure 8 shows that the dynamics of the power in the secondary beams (hence also in the primary beam) followed an exponential rise and fall with a time constant of 50 μs . At time $t = 0$ s, the micromirror corresponding to the 776 nm line was switched “on,” while the micromirror corresponding to the 780 nm line was switched “off”. At time $t = 1.5$ ms the reverse switching occurred. The characteristic rise and fall time is caused by the mechanical response time of a micromirror upon switching between two states.

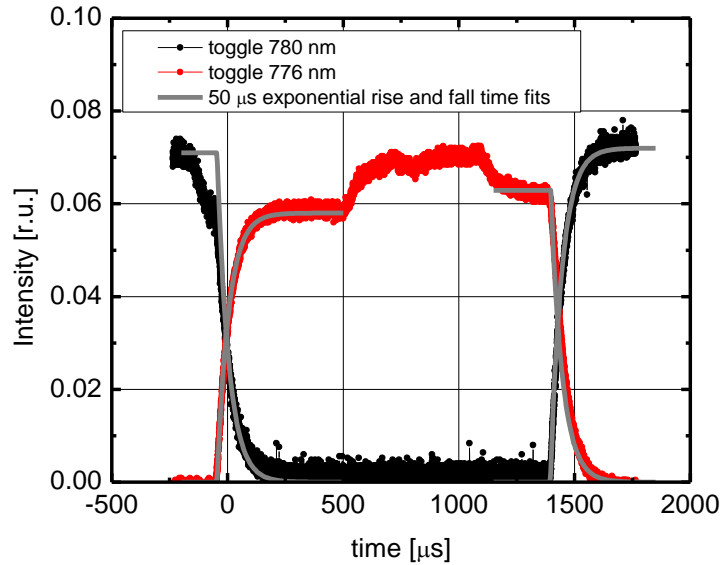


Fig. 8. Wavelength switching dynamics.

After 185 μs , the output power of the laser reached 99% of its maximum power. Therefore, the maximum switching rate of the laser is $1/1.5$ ms = 0.66 KHz, and 185 μs is the time necessary to fully switch on or off a wavelength.

At maximum switching rate, the laser responded very well as Fig. 9 illustrates.

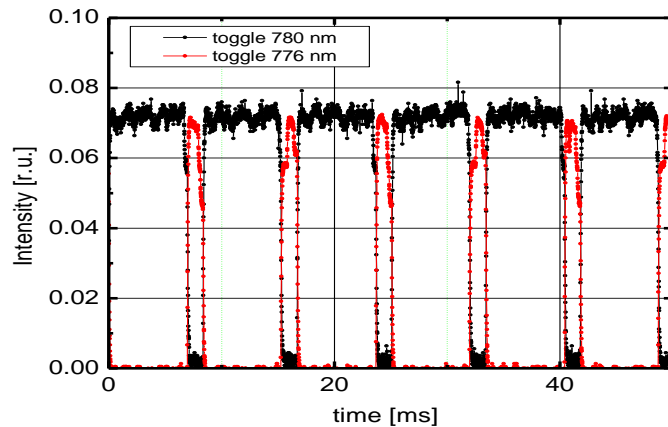


Fig. 9. Switching between two wavelengths at maximum switch rate of 0.66 kHz.

5.2 Wavelength switching repeatability

The repeatability of the absolute wavelength after multiple switching events was investigated. The power of the primary beam was measured by a wavelength meter (Coherent Wavemaster[®]) over a 4-second period (the necessary integration time of the instrument). Then, the laser was switched to a different wavelength and another 4-second period was held for measuring the wavelength. The process was repeated for multiple cycles. To illustrate this methodology, the left side of Fig. 10 shows the results of the measurement over a few initial cycles, with long term performance shown on the right. Channel 1 showed multiline operation for a short time (gap in data).

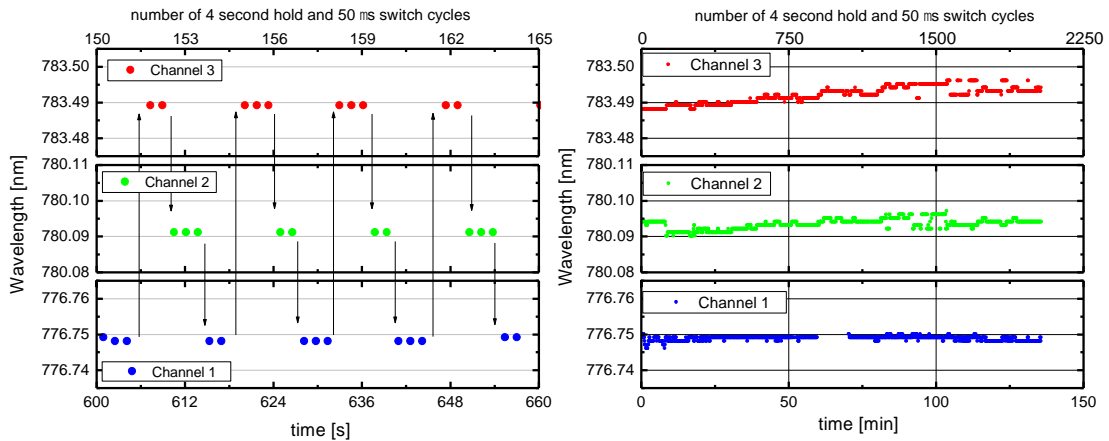


Fig. 10. Absolute wavelength measurement of switched wavelengths.

The measurement was run over a 2.5 hour period, representing ~ 2300 switching cycles. The results of this test are shown in Table 2. Standard deviation was calculated for single line measurements (thus excluding the gap in single line data in channel 1). Although the standard deviation increases with increasing wavelength, it is believed to be coincidental.

Table 2. Long Term Wavelength Performance of Wavelength Switching Operation.

	Average wavelength [nm]	Standard deviation [pm]
Wavelength 1	776.749	0.5
Wavelength 2	780.094	1.5
Wavelength 3	783.492	2.3

As a baseline comparison, when the laser is operated at one wavelength without switching, a wavelength drift of $\sim \pm 1$ pm is observed due to the thermal and current fluctuations. Thus, this performance demonstrates that the wavelength switching operation does not impact the absolute wavelength, when temperature and current fluctuations are taken into consideration. This is a remarkable result, demonstrating the excellent repeatability of the switching function.

6. Prospects

In this section, we discuss the envelope of tunable laser parameters that could be realistically obtained by pushing the technology, and its potential for use in THz applications.

One of the limiting factors in this tunable laser architecture is the number of gratings that can be multiplexed in a bulk photothermal holographic glass, since the number of multiplexed gratings corresponds to the number of discrete laser frequencies that could be accessed. Experimentally, the minimum diffraction efficiency of each grating was determined to be at least 25%, in order to provide sufficient feedback to the laser after double diffraction (50%

grating efficiency was used in the experiments, although 25% would have been also possible). The maximum refractive index contrast and the grating length determine the maximum number of multiplexed gratings that can be recorded, and thus the maximum number of switchable wavelengths in the laser. The index contrast Δn of each individual grating recorded sequentially is equal to $\Delta n = \Delta n_o/N$, where N is the number of multiplexed gratings and Δn_o is the saturation value of index contrast. For a thick phase reflection grating, the diffraction efficiency is given by [18]:

$$\eta = \tanh^2\left(\frac{\pi \cdot \Delta n \cdot t}{\lambda}\right),$$

where t is the length of the grating and λ the wavelength. The saturation refractive index change is $\Delta n_o = 1.5\text{E-}3$. However, the saturated refractive index change introduces high scattering losses in the near infrared. At 780 nm, the maximum index of refraction change that provides less than 10% loss due to scattering is approximately $8\text{E-}4$. This value is smaller than the maximum saturation refractive index change of the glass holographic material. Under this condition we can assume that the local refractive index change is proportional to the local light intensity. The modulation degree of the intensity pattern is therefore equal to the modulation degrees of the refractive index patterns.

A minimum grating length of approximately 3 mm is required to obtain single mode operation. The index of refraction modulation required to obtain an efficiency of 25% with $t = 3 \text{ mm}$ can then be computed from the diffraction efficiency relation above, which yields $\Delta n = 4.5\text{E-}5$. Thus, the expected maximum number of multiplexed gratings with 25% efficiency is $\Delta M = 8\text{E-}4/4.5\text{E-}5 = 17$ for a grating of 3 mm in length. By scaling the length t of the grating, the number of lines (i.e. wavelengths) can be further increased. For example, a VHG with 5 mm length could provide 29 multiplexed gratings, and a 6.2 mm long VHG could provide 40 multiplexed gratings, each with 25% efficiency.

A second potential limitation of this architecture is related to the focusing lens L2 in Fig. 1. If the incidence angle of the diffracted beam on lens L2 is too large, then the beam reflected by the micromirror will clip the aperture resulting in a low optical feedback and unstable laser operation. An estimate of the maximum incidence angle is given by Fig. 4, which shows that up to 2 degrees deviation from the lens optical axis provides adequate feedback for single mode operation. Therefore, the maximum angular span is 4 degrees (± 2 degrees). The minimum physical separation at the focal plane of lens L2 is constrained by the pixel size, which is $10 \mu\text{m}$ for the DLP micromirror array in the experiment. In terms of angular separation at lens L1, this translates to 0.065 degrees. Thus, the maximum number of wavelengths limited by the focusing length L2 is approximately 60 ($4.0/0.065$).

As mentioned in the introduction, this tunable laser possesses the required features for an efficient, fast, discrete-frequency-swept Terahertz source. The efficiency of photomixing for Terahertz generation is most favorable when two colors emitted from the same laser operate in single mode and are synchronous [6, 19, 20]. The number of discrete Terahertz frequencies that can be generated by this single tunable laser is computed by counting the number of unique two-wavelength combinations in a series of M wavelengths. The total number of possible discrete Terahertz frequencies given a tunable laser with M discrete wavelengths is $0.5 \cdot M \cdot (M-1)$.

The minimum Terahertz frequency is determined by the minimum spectral separation between two wavelengths, i.e the bandwidth of the VHG. Table 2 below gives the tunable laser parameters that can be obtained for different grating lengths t . The sweeping time for spanning the spectral range is given by the product of the number of discrete Terahertz frequencies and the minimum switching time of the DLP (1.5 ms).

Table 3. Summary of Expected Laser Characteristics Based on Different Volume Grating Lengths.

VHG length (t)	Maximum # wavelengths (M)	# discrete THz frequencies	Minimum THz frequency generated by one laser	Sweeping time
mm			GHz	ms
3	17	136	40	204
5	32	406	29	609
6.2	40	780	19	1170

For Terahertz imaging applications, the spectral range of interest is from 100 GHz to several THz. In practice, for low power lasers, the maximum Terahertz frequency that can be generated is determined by the bandwidth of the semiconductor photomixer which is currently limited to about 2 THz @ -3dB. Progress in advanced materials for photomixing might promise larger bandwidth. For comparison, the gain bandwidth of the semiconductor laser is 14 THz. The spectral range for imaging applications can therefore be achieved with the proposed single tunable laser.

For high-resolution Terahertz spectroscopy applications, Gigahertz resolution is desired [21, 22]. Although Gigahertz resolution cannot be practically achieved with the single tunable laser proposed, it would be possible to reach Gigahertz resolution by photomixing two lasers, one of which (or both) is the proposed discretely tunable laser. Further, this solution provides more frequency agility over current commercial high-resolution Terahertz systems using two thermally tuned DFB lasers that utilize continuous wavelength tuning [23, 24]. The proposed laser can access any sequence of discontinuous frequency points, in any order, without needing to tune continuously in a sweep from one frequency to the other thus avoids tuning across undesired frequencies. The DLP laser settling time is also small compared to the acquisition/detection time between switching (0.185 ms vs 1.5 ms), whereas the effective acquisition time at fixed frequencies for thermally tuned systems is dependent on the wavelength tuning speed.

Additional applications for the use of this fast discrete tunable source include three-dimensional imaging with digital holography [25, 26].

7. Concluding remarks

We have successfully demonstrated a prototype compact tunable laser, which produced single and multi-line operation in the near infrared with 37 mW output power while maintaining single mode output. The discrete wavelength switching capability uses a DLP micromirror array that has a turn on/off time constant of 50 μ s and switching rate of 0.66 KHz. The prototype laser has a size of 3x3x3 cm³. This combination of features in a single compact laser is unique and enabled by the multiplexed volume grating and a digital DLP micromirror array.

Features such as dual line single mode operation from a single laser, high power, fast tuning and sub-100 GHz frequency difference, in a compact form factor has, to the authors' knowledge, not been possible with other existing technologies. The characteristics of this laser are well suited for generating continuous-wave tunable Terahertz radiation with a single laser for imaging applications, and three-dimensional imaging with digital holography.

Acknowledgements

We acknowledge financial support from the National Science Foundation under Small Business Innovative Research grant # 0956430. We also thank Ron Logan, Emcore Corp. and Randy Heyler, Ondax Inc. for helpful comments on the manuscript.